AD-A108 316 ACCUMETRICS CORP CAMBRIDGE MA F/G 14/2
APPLIED RESEARCH AND DEVELOPMENT OF FALLING-SPHERE DENSITOMETER--ETC(U)
AUG 81 D H FRYKLUND F1962R-79-C-0058
UNCLASSIFIED AC-267 AFGL-TR-81-0233 NL

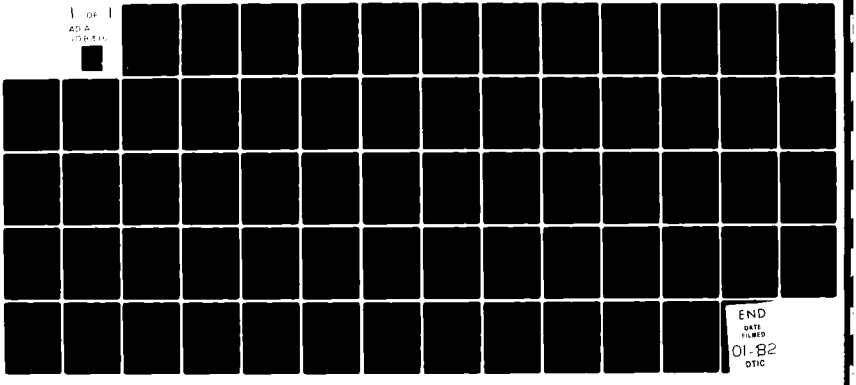

END
DATE FILMED
01-82
DTIC

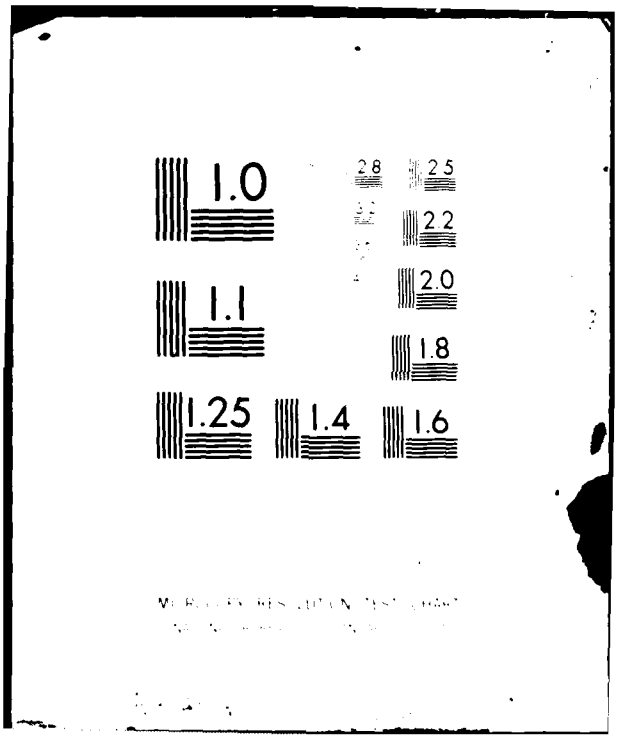
1.0
1.1
1.25
1.4
1.6
1.8
2.0
2.2
2.5
2.8

LEVEL II

12

AFGL-TR-81-0233

APPLIED RESEARCH AND DEVELOPMENT OF FALLING-SPHERE DENSITOMETER PAYLOADS OF IMPROVED DESIGN

Donald H. Fryklund

Accumetrics Corporation
344 Rindge Avenue
Cambridge, Massachusetts 02140

12 66

August 1981

Final Report for Period 79 January to 81 August

Approved for Public Release, distribution unlimited

AIR FORCE GEOPHYSICS LABORATORY
AIR FORCE SYSTEMS COMMAND
UNITED STATES AIR FORCE
HANSCOM AFB, MASSACHUSETTS 01731

404 121

Unclassified

SECURITY CLASSIFICATION OF THIS PAGE *(When Data Entered)*

REPORT DOCUMENTATION PAGE	READ INSTRUCTIONS BEFORE COMPLETING FORM
1. REPORT NUMBER: AFGL-TR-81-0233	2. GOVT ACCESSION NO.: AD-A108 316
3. RECIPIENT'S CATALOG NUMBER:	
4. TITLE *(and Subtitle)*: APPLIED RESEARCH AND DEVELOPMENT OF FALLING-SPHERE DENSITOMETERS PAYLOADS OF IMPROVED DESIGN	5. TYPE OF REPORT & PERIOD COVERED: Final Report 79 January-81 August
	6. PERFORMING ORG. REPORT NUMBER: AC-267
7. AUTHOR(s): Donald H. Fryklund	8. CONTRACT OR GRANT NUMBER(s): F19628-79-C-0058
9. PERFORMING ORGANIZATION NAME AND ADDRESS: Accumetrics Corporation, 344 Rindge Avenue, Cambridge, Massachusetts 02140	10. PROGRAM ELEMENT, PROJECT, TASK AREA & WORK UNIT NUMBERS: 62101F, 669004AE
11. CONTROLLING OFFICE NAME AND ADDRESS: Air Force Geophysics Laboratory, Hanscom AFB, Massachusetts 01731, Monitor: J. McIsaac/ LKB	12. REPORT DATE: August 1981
	13. NUMBER OF PAGES: 63
14. MONITORING AGENCY NAME & ADDRESS *(if different from Controlling Office)*	15. SECURITY CLASS. *(of this report)*: Unclassified
	15a. DECLASSIFICATION/ DOWNGRADING SCHEDULE

16. DISTRIBUTION STATEMENT *(of this Report)*

Approved for public release; distribution unlimited

17. DISTRIBUTION STATEMENT *(of the abstract entered in Block 20, if different from Report)*

18. SUPPLEMENTARY NOTES

19. KEY WORDS *(Continue on reverse side if necessary and identify by block number)*

Piezoelectric
Accelerometer
Densitometer
Transducer
Aeronomy
Atmospheric Density

20. ABSTRACT *(Continue on reverse side if necessary and identify by block number)*

Four complete falling-sphere densitometer systems were designed and fabricated, and were launched, with generally satisfactory results, at three locations: New Mexico, Sweden, and Alaska. The task included the provision and launch responsibility for the nose cones and ejection systems for all densitometers and the provision and launch and launch responsibility for two unique support units for the payloads flown in Sweden.

DD FORM 1 JAN 73 1473

Unclassified

SECURITY CLASSIFICATION OF THIS PAGE *(When Data Entered)*

cont.) →

In the on-going effort to improve system accuracy, refinements were made in the calibration and data reduction techniques for the Z-axis channels of the sphere. The Z-axis amplifiers have been modified to improve their performance. A general program to improve the system accuracy has been continued.

A wide-band accelerometer ~~has been~~ was designed and integrated into the sphere system to provide for a high resolution instrument to enable small-scale wind and turbulence studies of the high-altitude atmosphere.

The sphere has been reintegrated to provide for a more powerful transponder and a PCM-ranging system. A study was made to reassess the sphere configuration to reduce its gross weight. Design changes ~~were evolved which~~ will reduce this weight by 1 lb. Additional volume was recovered for future expansion in the sphere instrumentation.

FOREWORD

This document is the final report required under Contract No. F19628-79-C-0058 to perform engineering research and development to evolve, fabricate, test, and calibrate falling-sphere densitometer payload systems of improved design.

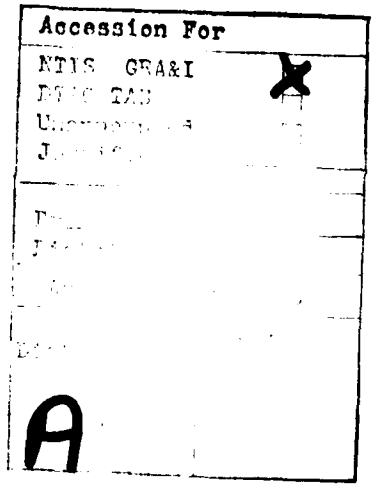

TABLE OF CONTENTS

LIST OF FIGURES

NOMENCLATURE

a	Acceleration, instantaneous
A	Acceleration, peak or steady-state
A	Area
C	Capacitance, farads, microfarads
d	Distance
e	Emf, volts, instantaneous
E	Emf, volts, peak or steady-state
ε	Dielectric constant
F	Force
f	Frequency, Hz
G	Piezoelectric constant
g	Acceleration due to gravity
K	Spring constant
K'	Effective Gain
K	Gain
L	Length
m	Mass
R	Resistance, ohms
R	Radius
r	Radius
t	Time, seconds
t	Thickness

T	Time constant
v	Voltage, instantaneous
V	Voltage, volts, peak or steady-state
x	Distance, instantaneous
X	Distance, steady-state
ω	Frequency, angular velocity, radians/second
ω_n	Natural angular frequency, zero-g
ω_{nT}	Natural angular frequency, test, sea level
ω_{ns}	Natural angular frequency, flight
ω_s	Spin angular frequency
ζ	Damping ratio

I. INTRODUCTION

Four densitometer systems complete with nose cones and sphere ejection systems where provided under this contract. The component parts of two nose-cone and ejection systems were provided by AFGL as GFE; the other two systems were manufactured from AFGL-furnished drawings that were modified and up-dated. Additionally, two support systems, unique to the sphere payload, were designed and fabricated. These were in the form of 12-inch long extension cans which were secured to the bottom end of the sphere portion of the payloads.

Support was provided for three field trips: White Sands Missile Range, New Mexico, where densitometer AC-11 was launched but failed to attain altitude because of a failure in the second-stage rocket; Esrange, Kiruna, Sweden, where densitometers AC-12 and 13 were launched; and Poker Flat Rocket Research Range, Fairbanks, Alaska, where densitometer AC-14 was launched. Satisfactory performance was achieved with the last three systems.

The special support systems (mini-support units) provided only the pyrotechnic timers and power supplies for the nose-cone and sphere ejection systems, and provision for the main umbilical cable. The sensors and TM link

normally provided in this section for monitoring rocket performance could be eliminated because this information can be derived from the sphere sensor system and TM link.

To improve the resolution of the densitometer for the study of high-altitude winds and turbulence three of the systems were implemented with wide-band accelerometers. These units were designed, fabricated, and calibrated, and were integrated into the spheres with their sensitive axes aligned with the sphere spin axes.

The effort under the contract included the re-design of the Z-axis chain of the sphere system to improve its performance. Additionally, as a continuing effort to improve the measuring accuracy of the sphere system, new techniques were developed for the calibration of the transducers and amplifiers, and several techniques were evolved to facilitate the calibration and data reduction of the Z-axis chain.

The sphere had to be re-integrated to accommodate the new higher-powered transponder and the OSURF PCM-ranging system. Because these systems are flown separately depending upon ground support radar facilities, two configurations had to be evolved. Relative to this effort was a study to reassess the sphere design with the aim of achieving sphere weight reduction. A new configuration was developed involving few basic changes in the existing configuration which will reduce the weight by 1 lb. Corollary

to this study was the securing of additional unused volume which may be used for future expansion of the sphere instrumentation.

II. Z-AXIS CALIBRATION AND DATA REDUCTION

2.0 General

Calibration and data reduction procedures are more complex for the Z-axis than the X and Y axes because this axis does not have a spin modulated input. Spin modulation allows the application of straight-forward steady-state sine-wave techniques at frequencies easily generated and measured. The signal generated by the Z-axis transducer closely approximates a slowly varying exponential time function whose Fourier components involve very low frequencies.

The use of an accelerometer that would have a response flat or uniform down to zero, or nearly zero frequency would simplify the calibration and data reduction task. Such an accelerometer would have a complex transducer which would be difficult to locate at the sphere mass in the presence of the X and Y transducers which must share this same position. It has been decided that the Z-axis system should be kept in its present simple design by trading off this more reliable system for more complexity in the post-flight data reduction.

2.1 Error Analysis

As shown in Figure 1 the electrical equivalent of the

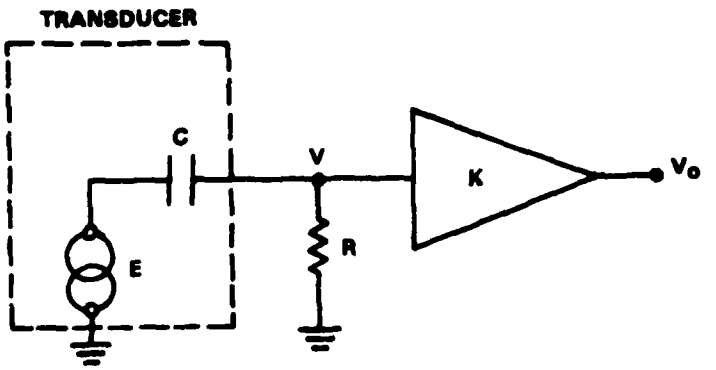

Transducer Equivalent Circuit

FIGURE 1.

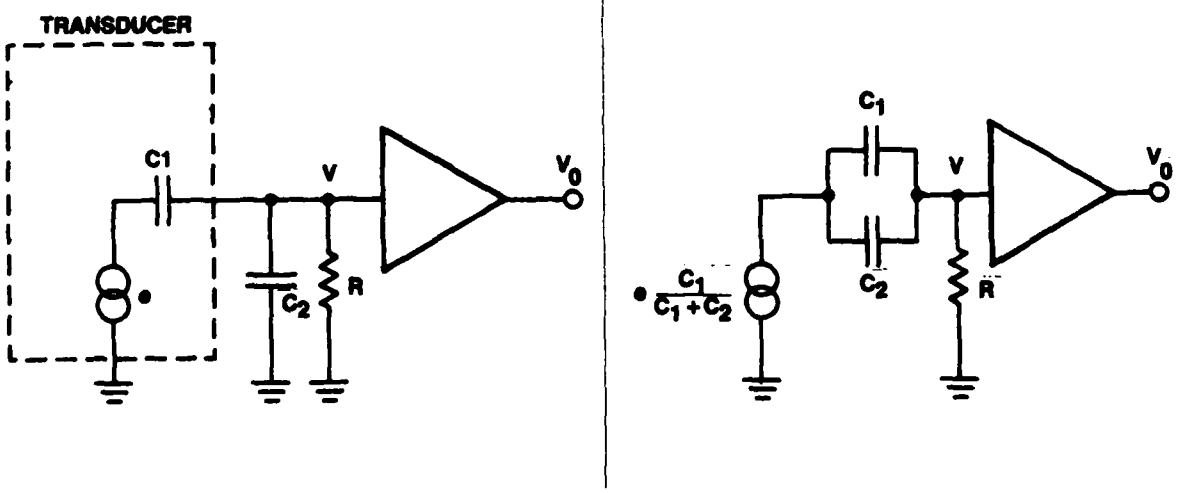

Shunted Input and its Equivalent

Figure 2

piezoelectric bimorph transducer is inherently a voltage generator connected to a series capacitance which in turn connects to the input resistor of the amplifier. Thus, it is seen that as the signal frequency decreases the attenuation increases by 6 db per octave and the transducer will not pass a steady-state voltage to the amplifier input. This is not an important constraint with regard to the X- and Y-axis amplifiers because the information involving these axes is carried on the sphere spin frequency (5-6 Hz). However, because the Z-axis data is not spin modulated and even though the Z-axis drag acceleration signal is not steady-state but is an exponentially-varying function, the signal attenuation due to the inherent RC coupling of the bimorph must be considered.

The loop equation for the input circuit of Figure 1 is

$$e = \frac{1}{C} \int idt + Ri$$

and since $v = Ri$

$$e = \frac{1}{RC} \int vdt + v \qquad (1)$$

and because $v_0 = Kv$

$$e = \frac{1}{K}\left[\frac{1}{RC} \int v_0 dt + v_0\right]. \qquad (2)$$

It is seen from the above that the circuit will pass any time function with minimum distortion provided that

$$\frac{1}{RC}\int v_0 dt \ll v_0 \qquad (3)$$

The first term in Equation 2 can be considered as an error in the analog signal. To minimize this error the RC product should be made as high as practicable.

The size of the input resistance R is limited by the noise voltage it generates, both due to thermal effects and semi-conductor input (gate) leakage current. The capacitance C (Figure 1) is limited by the inherent internal capacitance formed by the required transducer element configuration. However, the effective capacitance may be increased by a proportional sacrifice in transducer sensitivity by the use of a shunt capacitance as shown in Figure 2. This is demonstrated by the use of steady-state sinewave analysis. Because the RC network is passive and linear the resulting input sensitivity and time constant modifications will be the same for the transient response of the network.

The voltage v is given by

$$v = \frac{Re}{1 + j\omega RC_2} \times \frac{1}{\frac{1}{j\omega C_1} + \frac{R}{1 + j\omega RC_2}}$$

$$= \frac{e}{\frac{1}{j\omega RC_1} + \frac{C_2}{C_1} + 1}$$

$$= \frac{C_1}{C_1 + C_2} \times \frac{e}{1 + \frac{1}{j\omega R(C_1 + C_2)}} \qquad (4)$$

Setting C_2 to zero in Equation 4 gives the solution for

the circuit of Figure 1:

$$v = \frac{e}{1 + \frac{1}{j\omega RC}}$$

Thus, it is seen that the shunt capacitor, while reducing the sensitivity by the factor $C_1/(C_1 + C_2)$, will increase the time constant in Equation 2 by a factor of $(C_1 + C_2)/C_1$. This technique is used in both the Z-axis amplifier and mutation sensor amplifiers. It should be pointed out that the incorporation of the shunt capacitor C_2 does not alter the single-time-constant nature of the circuit.

Additionally, it should be pointed out that the shunt capacitor has no affect on the signal-to-noise ratio of the amplifier as the capacitor voltage division operates on the signal and noise voltages equally.

The error term in Equation 2 can be examined by its evaluation with the function

$$v_0 = V(e^{t/T} - 1) \tag{5}$$

which closely approximates the down-leg Z-axis analog output voltage of the densitometer system. Thus

$$\frac{1}{RC}\int v_0 dt = \frac{1}{RC}\int V(e^{t/T} - 1)dt$$

$$= \frac{1}{RC}\left[VTe^{t/T} - Vt + c\right]$$

c is evaluated by observing that $v_0 = 0$ when $t = 0$, therefore

$$c = -VT$$

and the error term, Equation 2, becomes

$$\frac{T}{RC}\left[V\left(e^{t/T} - 1\right) - \frac{Vt}{T}\right] \tag{6}$$

Division by v_0 will yield the fractional error in the output of the network as a function of time

$$\frac{\frac{1}{RC}\int v_0 dt}{v_0} = \frac{T}{RC}\,\frac{V(e^{t/T} - 1) - Vt/T}{V(e^{t/T} - 1)}$$

$$= \frac{T}{RC}\left[1 - \frac{t}{T(e^{t/T} - 1)}\right] \tag{7}$$

Equation 7 may be examined by taking its limit by application of L'Hopital's Rule to obtain the limit of the second term:

$$\lim_{t\to a} \frac{t}{T(e^{t/T} - 1)} = \lim_{t\to a} \frac{1}{e^{t/T}}$$

For which when $t/T \ll 1$ closely equals unity, and for $t/T \gg 1$ approaches zero. Thus, from Equation 7 for small t/T the error in the analog signal will be zero (or small). For large t/T the error will approach

$$\frac{T}{RC}$$

For the Z-axis amplifier the RC time constant is 33 seconds and, typically, the time constant T of the down-leg data is 4 seconds. The measuring interval for any of the

Z-axis channels is 20 seconds or less. Evaluation of Equation 7 with these quantities yields a fractional error in the analog data of 0.117 so that the fractional error range will be

$$0 \leqslant \frac{dv_0}{v_0} \leqslant 0.117$$

corresponding to the time range of $0 \leqslant t \leqslant 20$ seconds. Thus, it is seen that if the first term of Equation 2 is ignored, the Z-axis output will be essentially the true analog of the input signal for small t, and after a period of 20 seconds the error will integrate to cause the calculated input voltage to droop and depart from being the true analog of acceleration by 11.7%.

The foregoing applies to the nutation sensor data except that the RC time constant and measuring interval are both smaller, and hence, the error will be different.

2.2 Data Reduction by Direct Integration

It is seen from Equation 2 that for any RC product the true analog voltage e can be recovered by adding the quotient of the time integral of the output voltage and time constant to the output voltage by means of a computer. Since the output voltage is telemetered, this operation can be done with a general-purpose computer on the ground. As with all the following compensation techniques, any residual offset voltage must be subtracted from the flight data before integration.

2.3 Analytic Methods

Flight data compensation may be performed graphically or analytically to reduce the error discussed above to within the accuracy of the best fit obtainable of the function

$$v_0 = V(e^{t/T} - 1) \tag{8}$$

to the flight data. The accuracy may be improved by a piece-wise succession of fits using this function but with different time constants; with each function covering a fraction of the total time interval. Thus, accuracy is improved both by obtaining a closer fit and by reducing the time interval covered by each function with its attendant reduction, as discussed above, in integrated error. For example, if the 20 second interval used above is divided into four 5-second intervals evaluation of Equation 7 with $t = 5$ gives a maximum error of 6% as compared to the 11.7% error corresponding to the full 20 second interval.

An alternate technique, involving the compensation for the error term in Equation 2 again uses the best fit of the function, Equation 8, to the flight data. Evaluating Equation 2 with Equations 5 and 6 gives

$$e = \frac{1}{K}\left\{\frac{T}{RC}\left[V(e^{t/T} - 1) - \frac{Vt}{T}\right] + V(e^{t/T} - 1)\right\}$$

$$= \frac{VT}{KRC}(e^{t/T} - 1) + \frac{V}{K}(e^{t/T} - 1) - \frac{V}{KRC}\,t \tag{9}$$

which by inspection suggests the following data reduction procedure:

1. Subtract off the off-set voltage from the flight data.
2. Determine best fit curve to match the flight data of the form $V(e^{t/T} - 1)$. Divide this by the measured amplifier gain K (the gain obtained by the sinewave calibration of the amplifier) to obtain curve A, Figure 3.
3 Determine curve B by multiplication of curve A by the factor T/RC.
4. Determine curve C by multiplying the Abscissa values by the factor $(-V/KRC)$.
5. Add curves A, B, and C to obtain curve D, the transducer analog voltage.

Further improvement in the data reduction accuracy will result if this technique is applied by piece-wise fitting of the function $V(e^{t/T} - 1)$ where T is adjusted separately for several functions each covering a smaller and successive portion of the total time interval of measurement, as discussed earlier.

2.4 Data Reduction by Means of Direct Calibration

Because the down-leg time function of drag acceleration is closely approximated by the function given by Equation 5 a function generator has been designed and built which produces this function with selectable time constants. This system is described in detail in report No. AFGL-TR-79-0101.

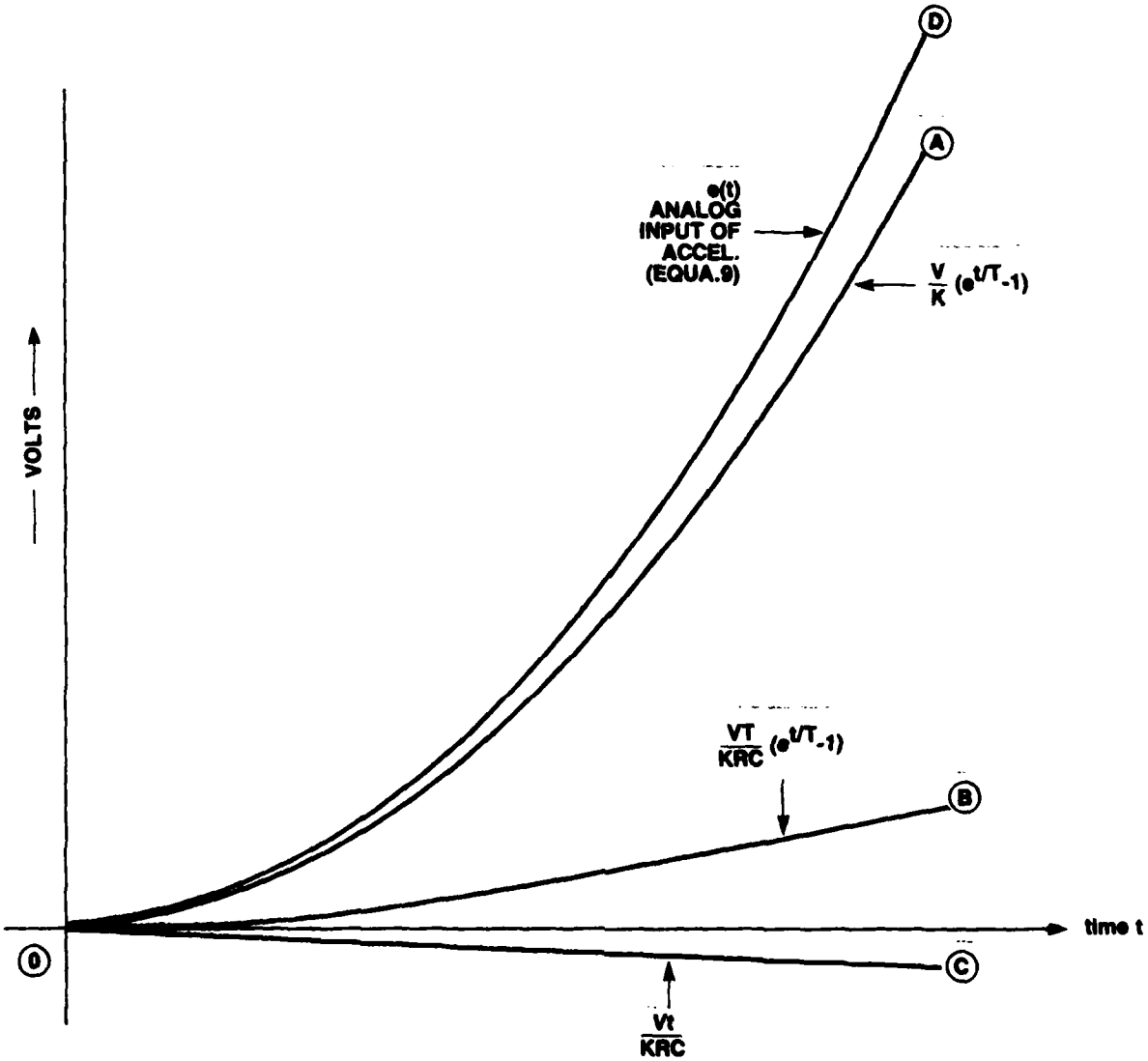

Z—axis Response Compensation

Figure 3

The preceeding reduction techniques require that the amplifiers have only one RC time constant. The direct calibration technique does not impose any constraint on the nature of the amplifier networks.

By the use of this generator the Z-axis amplifier chain is directly calibrated to produce a family of response curves, each curve having a different time constant so that the family of curves will bracket the predicted range of time constants of the flight data. The data reduction procedure then is as follows:

1. Subtract off any residual off-set voltage from the flight data.
2. Determine the time constant(s) T for the down-leg data.
3. Select from the calibration curves the curve(s) which match(es) the flight data time constant(s). This may require interpolation of the calibration data to obtain the curve(s) having the best match.
4. A single curve, or a piece-wise fit, as discussed earlier, of several curves may be used.
5. From the selected calibration curve(s) determine the effective amplifier gain K' by dividing the output curve(s) by the corresponding input curve(s). The effective gain K' will be a function of time.
6. Divide the flight data by the gain function K' to obtain the input analog function of acceleration.

Because the foregoing procedure involves the matching of time constants it is of interest to examine the influence of the error in the time-constant match upon the determination of the input analog function.

The evaluation of Equation 2 with the function of Equation 5, and with the input function generated by the special function generator, viz

$$e = E(e^{t/T} - 1)$$

the following is obtained

$$E(e^{t/T} - 1) = \frac{1}{K}\left[\frac{V}{RC}(Te^{t/T} - t - T) + V(e^{t/T} - 1)\right]$$

from which one obtains

$$K' = \frac{V}{E} = \frac{K}{1 + \frac{T}{RC}\,\frac{e^{t/T} - t/T - 1}{e^{t/T} - 1}} \tag{10}$$

which for $t/T \ll 1$

$$K' = K \tag{11}$$

and for $t/T \gg 1$

$$K' \simeq \frac{K}{1 + \frac{T}{RC}} \tag{12}$$

For small t the selection of the best-fit calibration curve is not critical with respect to determination of the time constant T as is seen by Equation 11. For large t operations of differentiation and division on Equation 12 gives

$$\frac{dK'}{K'} = - \frac{1}{1 + \frac{RC}{T}} \frac{dT}{T}$$

Evaluation of this function for a typical system and flight where RC = 33 seconds and T = 4 seconds

$$\frac{dK'}{K'} = \frac{1}{1 + \frac{33}{4}} \frac{dT}{T} \approx 0.11 \frac{dT}{T}$$

If the error in the selection of T is 10% the error in the determination of the effective gain K' will be 1%.

III. Z-AXIS PERFORMANCE IMPROVEMENTS

3.0 General

The Z-axis component of acceleration is obtained from four channels, three from outputs taken off from the amplifier chain driven by the Z-axis transducer of the main accelerometer, and one from a separate transducer which has the additional function of measuring the free precession (nutational) motion of the sphere. These channels cover the following acceleration ranges:

Z_2 - 4×10^{-5} to 4×10^{-3} g

Z_3 - 4×10^{-4} to 4×10^{-2} g

Z_4 - 4×10^{-3} to 4×10^{-1} g

Z_5 - 5×10^{-2} to 2 g (also provides nutation data)

3.1 Circuit Changes

Because the main accelerometer proof mass centers cannot be bore-sighted exactly to coincide with the sphere mass center it will sense a small amplitude of nutational acceleration which occurs at a frequency close to 1 Hz. In earlier systems this interfering signal has been notched out by the use of a band-rejection filter centered at the nutation frequency and placed in the input of the Z-axis

amplifier chain. Data from successive flights have shown that notch filtering is required only in the most sensitive channel.

The Z-axis amplifier was redesigned to eliminate the notch filtering in all channels except the Z_2 channel, thus, all Z channels except the Z_2 channel have single time constants enabling the use of the data reduction techniques covered in the previous section. The Z_2 data recovery is limited to the function generator calibration technique because of the multiple-time-constant character of the notch filter.

Off-set drift in the Z-axis chain has been improved by a factor of ten by replacing the ZN5906/NA2-2725-5 amplifiers with the newly-developed AD515 amplifiers.

3.2 Natural Frequency Correction for Z_5 Transducer

The Z_5 data is obtained from a transducer positioned a calibrated distance away from the sphere mass center. This positioning is required so that the transducer will sense nutational acceleration. Multiplexing of nutational data with the air drag data is possible in this channel because the nutational acceleration comprises only a fraction of the drag acceleration range covered by this channel, and because of the frequency separation between these accelerations, the nutation being approximately a 1 Hertz sinusoid, and the air drag being a slowly changing exponential function.

The Z_5 or nutation sensor transducer natural frequency

must be corrected for the gravity stiffening that occurs during calibration as described in Report No. TR-79-0101. In addition, the natural frequency must be corrected for in-flight stiffening due to the spin induced centrifugal acceleration.

Referring to Figure 4, the spin induced centrifugal force is given by

$$F = MR\omega_s^2$$

A component of restoring force appears when the transducer is deflected by the small angle θ of

$$f = MR\omega_3^2\theta = MR\omega_s^2 \frac{z}{r}$$

so that the dynamical equation of forces, neglecting the damping forces which are small and negligible, will be

$$M\ddot{z} + \left(\frac{MR\omega_s^2}{r} + K\right)z = 0$$

from which it is seen that

$$\omega_{ns} = \left(\frac{R}{r}\omega_s^2 + \omega_n^2\right)^{\frac{1}{2}} \qquad (13)$$

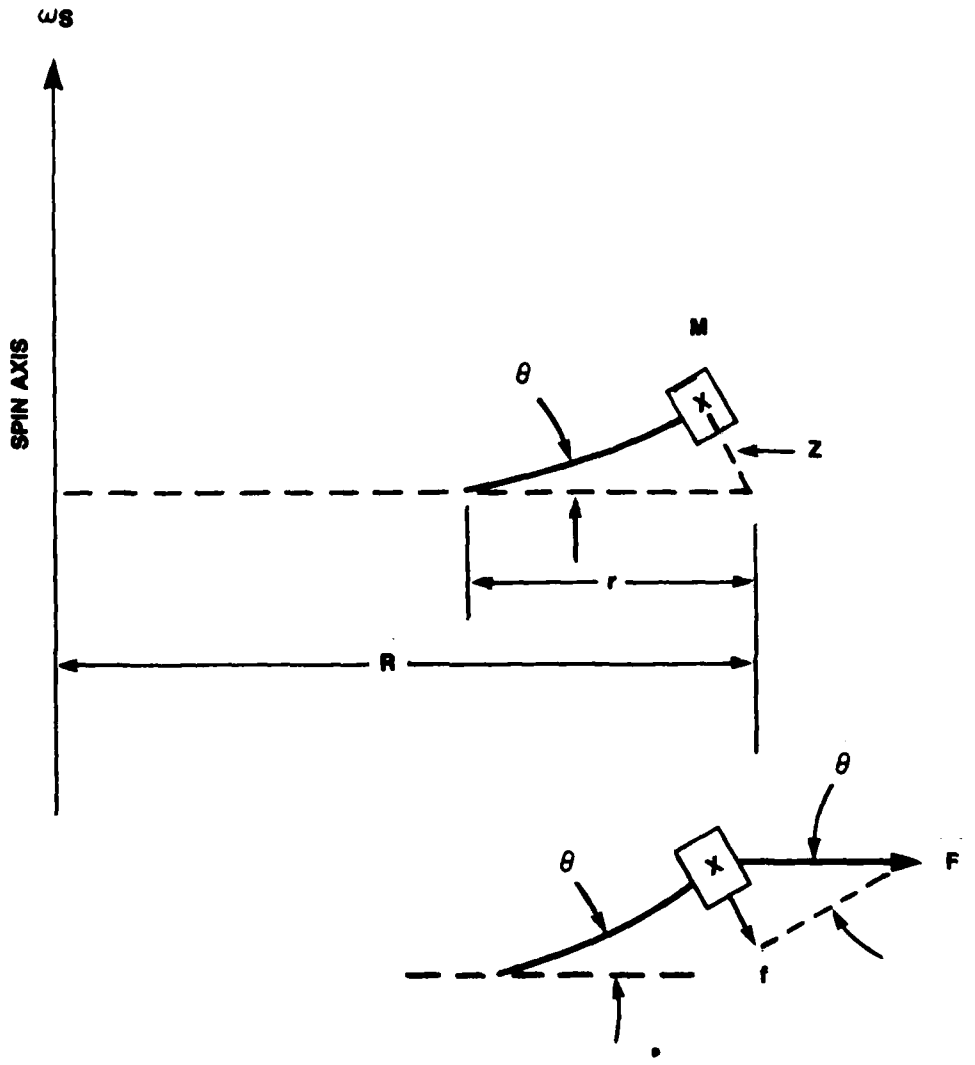

Spin Induced Restoring Force, Nutation Sensor, Z5
Figure 4

IV. CALIBRATION ACCURACY IMPROVEMENTS

4.0 General

In addition to the studies and improvements made in the accuracy of the calibration of the Z-axis and nutation sensor channels described in the preceeding section, a general assessment of techniques and procedures has been continuing in the improvement of the accuracy of calibration of the entire system. An improved technique has been evolved for the calibration of the transducer sensitivities, and a more precise method has been evolved for the measurement of transducer natural frequencies.

4.1 Transducer Calibration

In the past the transducers have been calibrated by driving the calibration fixture with an electromagnetic displacement generator. To provide for mechanical filtering to ensure pure sine-wave motion the fixture is tuned to the test frequency by the use of suitable ballast mass. Because the displacement generator is a spring-mass system with a low natural frequency, care had to be taken to reduce the coupling between the fixture and the generator to avoid the double-resonance characteristic of closely coupled resonant systems.

Decoupling between the test fixture and the generator

was accomplished by the use of a soft spring through which the generator transmits its force to the fixture. This resulted in a very slow flow of energy into the fixture for level changes of the generator causing long duration lags between input level settings and final displacement levels.

Because the fixture, without the generator coupled to it, has a very low damping coefficient, shock excitation causes a slowly decaying oscillation of approximately 15 seconds duration. Thus, if the fixture is displaced by an amount greater than the measuring range of interest the arrival of the displacement at the desired starting point is easily anticipated. This is true for each successive lower amplitude point. Thus, for one shock of the fixture a series of calibration points are obtained for different levels of displacement. The calibration technique was changed to use this free oscillation principle instead of the driven method. Results have proven that this technique is superior in that the data dispersion in successive calibration runs is much smaller.

A push-button switch has been provided at the microscope viewing position so that for each predetermined displacement level a mark can be recorded on the strip-chart.

Improvement in the measurement of the transducer natural frequency has been obtained by the implementation of a frequency counter system. In the past, because the

counter would quickly lose lock on the decaying damped wave from the shock excited transducer, this measurement was performed with a strip-chart recorder. By the use of a limiter circuit the damped wave is now clipped at a low level to produce a series of equal amplitude square waves. These square waves are then passed through a differentiating circuit after being amplified, the resulting spike wave train is then fed into the counter.

As a result of the transducer malfunction in sphere AC-14 the sequence of the transducer calibration is being changed. Because of the hazards resulting in the handling required by the natural frequency measurements the sensitivity calibration and capacitance measurements will follow those of the natural frequencies. In this manner any element fracture in handling will become apparent.

4.2 Amplifier Calibration

Calibration of the amplifiers has been improved by taking greater care in the procedures outlined in previous reports. More frequent checking of the system calibration and a greater number of repeats are being made. Studies in further improvement in the accuracy of the amplifier calibration suggest two improvements that will be made in the future.

The former procedure entailed the measurement of the transducer internal capacitance. This capacitance was then duplicated in value with a low-loss fixed capacitor which was used to couple the frequency generator to the

amplifier being calibrated. In the future the transducer will be used directly as the coupling capacitor for the low sensitivity ranges. The voltage division measured between the generator and the amplifier input will then be used to establish the proper size of the coupling capacitor which must be used for the higher sensitivity ranges. The direct use of the transducer for the coupling at higher sensitivities cannot be used because the transducer produces voltages due to seismic noise even though it is shock isolated with compliant padding.

Considerable improvement in the calibration of the amplifier chains can be realized by a potentiometic technique that has been designed. This is comprised of a decade potentiometer that will divide its input voltage to an accuracy of one part in one thousand. This is done with four identical decade resistance boxes each having ten positions made up with ten equally sized precision resistors having tolerances of 0.01%. The arm of the switch of one box is coupled to the input of the next box with a unity-gain operational amplifier to prevent the variable loading by the following box on the preceeding box. Three unity-gain isolation amplifiers would be required.

The amplifier output being calibrated would be fed to the input of this potentiometer system which in turn would feed the strip-chart recorder. The measurement procedure then would be to keep the recorder deflection constant at

nearly a full-scale level by switching the input potentiometer described above. The amplifier gain would then be the product of the fixed recorder indication and the potentiometer settings.

This technique would reduce reading inaccuracy experienced with strip-chart recorders especially at low deflection levels, and would eliminate any nonlinearity in the measuring system that may be present.

V. WIDE-BAND ACCELEROMETER

5.0 General

Flight data from prior flights have revealed that the main triaxial accelerometer will provide dynamic structural data of the atmosphere such as caused by winds, but because of the limited bandwidth of this accelerometer the resolution of the measurement of these finer-scale phenomena is limited. To facilitate this type of study a wide-band accelerometer has been developed and fabricated having a frequency response that is uniform over the range 10 Hz to 20 KHz, and which has a sensitivity of 10^{-4} to 10^{-6} g. This accelerometer was installed in the sphere with its sensing axis aligned with the spin axis so that its output is not spin modulated, and is therefore not constrained by the spin sampling rate with its attendant reduction in resolution.

The limited sensitivity range is the consequence of the TM channel capacity as the wide-band nature of the accelerometer data necessitated the use of a separate TM channel. The addition of another TM channel would increase the sensitivity range another two decades to give a range of 10^{-2} to 10^{-6} g.

5.1 Transducer Design

The general design equation for the piezoelectric accelerometer is

$$v = \frac{K\,a}{\omega_n^2}\left\{\left[1 - \left(\frac{\omega}{\omega_n}\right)^2\right]^2 + \left[2\,\frac{\zeta\omega}{\omega_n}\right]^2\right\}^{-\frac{1}{2}} \qquad (14)$$

where $0 < \zeta \leq 1$.

It is seen that if $\omega_n >> \omega$ this equation reduces to

$$v = K\,a/\omega_n^2 \qquad (15)$$

and for $\zeta = 10^{-2}$ and $\omega_n = 3\omega$ Equation 15 will be accurate to within approximately 9%. This error can be reduced by the adjustment of the damping ratio as can be seen by expanding the terms within the radical

$$\left[1 - \left(\frac{\omega}{\omega_n}\right)^2\right]^2 + \left[2\zeta\,\frac{\omega}{\omega_n}\right]^2 = 1 - 2\left(\frac{\omega}{\omega_n}\right)^2 + \left(\frac{\omega}{\omega_n}\right)^4 + 4\zeta^2\left(\frac{\omega}{\omega_n}\right)^2$$

If ζ is adjusted so that it is equal to 0.707 the above reduces to

$$1 + \left(\frac{\omega}{\omega_n}\right)^4 \simeq 1$$

Thus, if the natural frequency is set at 6 KHz and a damping ratio of 0.707 is provided, the transducer response will be flat out to 2 KHz. This high natural frequency requirement suggests the use of a very stiff piezo element configuration, i.e., a simple compression element instead of the usual bimorph bender.

Equation 14 shows that the voltage generated by the transducer will extend uniformly down to zero frequency.

However, because this voltage is coupled to the required amplifier and signal conditioner electronics by its internal capacitance the low frequency response of the transducer and amplifier will be limited by the amplifier input resistance and by the internal capacitance of the transducer element.

The amplifier input resistance is limited in its size by the noise it generates. This noise is partly due to thermal agitation but is largely due to semiconductor noise which is high in the very low frequency spectrum and decreases markedly along an exponential curve for increasing frequencies. This noise is proportional to the input (gate) resistance of the amplifier

$$e_n = BR \tag{16}$$

where B is a constant.

The low frequency voltage output of a piezoelectric compressor element can be expressed in terms of its thickness, area and piezoelectric constant as

$$v = G \frac{t}{A} Ma \tag{17}$$

and its capacitance as

$$C = \varepsilon \frac{A}{t} \tag{18}$$

Equation 17 can be written in terms of the capacitance parameter by elimination of the ratio t/A between Equations 17 and 18

$$V = G \frac{\epsilon}{C} Ma \tag{19}$$

The signal-to-noise ratio for the transducer is then given by Equations 16 and 19

$$\frac{V}{e_n} = \frac{G\epsilon}{BRC} Ma \tag{20}$$

It is seen from Equation 20 that in the design of the transducer a trade-off must be made between the low frequency roll-off and the signal-to-noise ratio. An increased RC time constant produces a decreased roll-off frequency at the low end of the transducer bandpass, but as observed from Equation 20, this will result in a reduced signal-to-noise voltage. Increasing the mass M in Equation 20 will off-set the increased RC time constant but this will result in decreasing the natural frequency of the transducer.

Trade-off studies using Equations 17 and 20 resulted in the selection of transducer elements of 0.28 inches diameter and 0.1 inches thick; having a capacitance of 680 pfd.

A proof mass of 100 grams is used as shown in Figure 5. Damping was accomplished by filling the space between the mass and the case with Dow-Corning 170 Silicone rubber. As shown in the figure, two elements are used in a parallel connection to facilitate the isolation of the high potential sides from ground. This configuration produces a sensitivity of approximately 1 v/g.

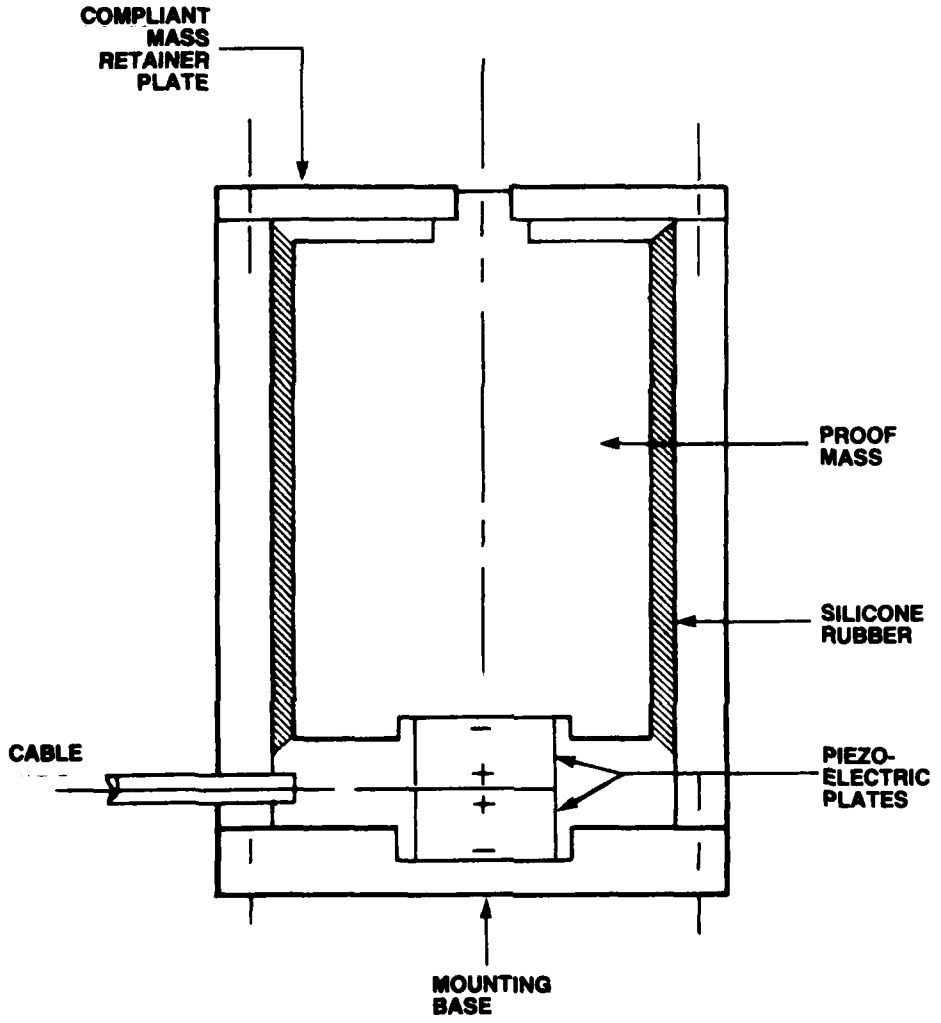

Wide-Band Accelerometer
Figure 5

5.2 Transducer Calibration

The wide-band accelerometer transducer is calibrated by the use of a sine-wave displacement generator that provides a moving table similar in configuration to the familiar vibration exciter used for vibration and shock testing. A spectrum analyser is used to make both level and response measurements. The table is calibrated by means of a standard accelerometer having a very high natural frequency which has been calibrated by means of a microscope.

Both the transducer and the standard are placed on the table and the frequency of displacement is swept over the spectrum of 10 Hz to 2 KHz. The output response curve is stored on the scope of the analyser. This is followed by the trace of the transducer response curve. With the two curves displayed on the scope the transducer can be readily calibrated over its frequency range by observing the difference between the curves in decibels and by applying this quantity to the sensitivity of the standard.

5.3 Amplifier Design

Figure 6 depicts the schematic of the amplifier and signal conditioner electronics. The amplifier provides sufficient gain to produce a ± 2.5-volt signal to the signal conditioner system for an input acceleration of 10^{-6} to 10^{-4} g. The signal conditioner provides a stable +2.5 volt zero thereby off-setting the amplifier signal to present a 0.05 to 5-volt input to the TM system. Additionally, the signal conditioner provides signal limiting so that the voltage

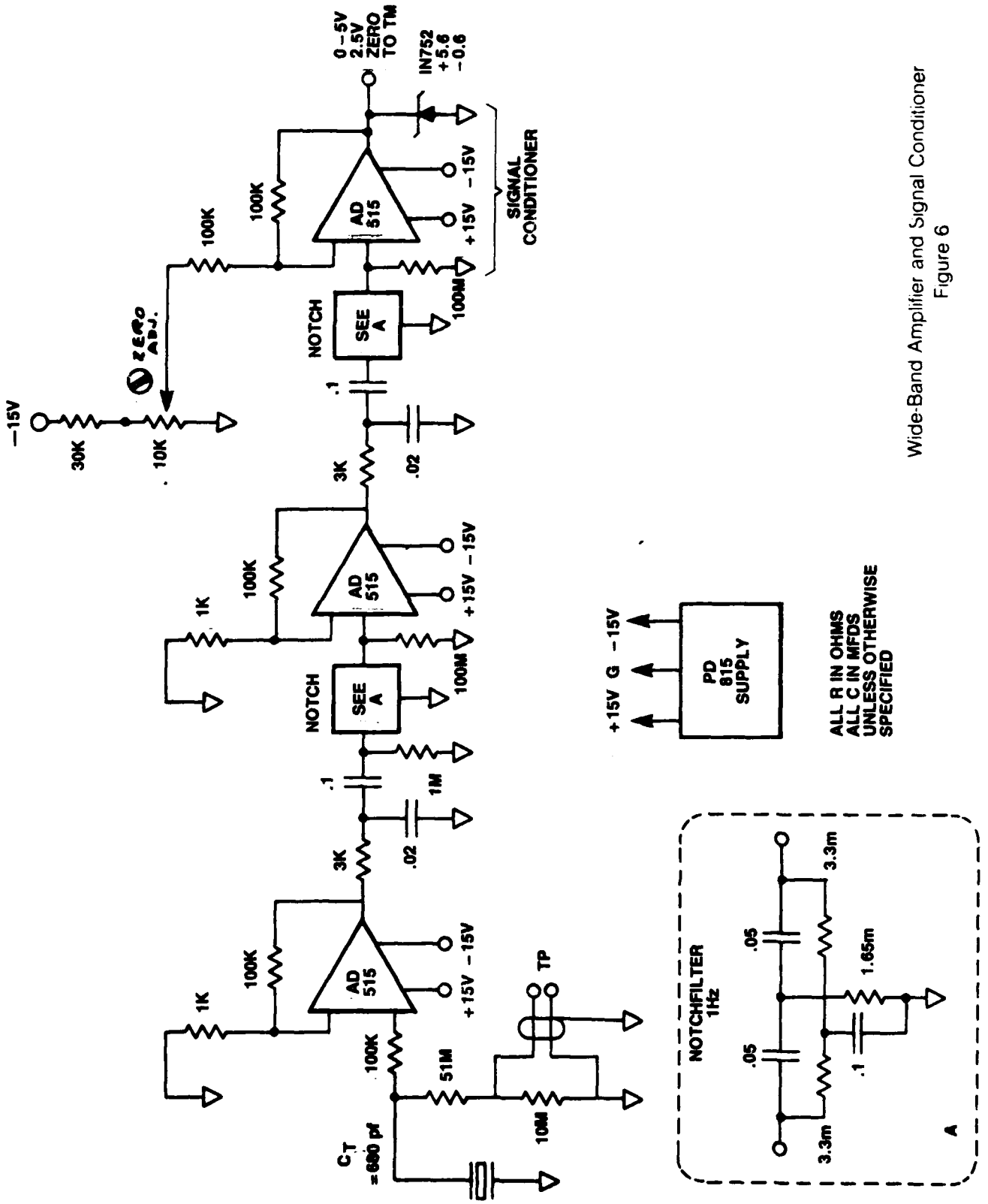

Wide-Band Amplifier and Signal Conditioner
Figure 6

supplied to the TM system cannot exceed the range $-0.6 \leq V_{TM} \leq +5.6$ volts.

The amplifier shown in Figure 6 provides a gain of 2.5×10^4 along the flat portion of the frequency response curve. Six decibel/octave roll-off results at the low end and high end of the spectrum due to the transducer internal capacitance, and the two 0.02 mfd shunt capacitors, respectively.

Because the wide-band transducer cannot be placed at the mass center of the sphere (occupied by the main accelerometer) it will sense a considerable component of nutational acceleration. The low frequency roll-off at the nutation frequency is approximately 12 db which represents insufficient attenuation to reduce this interference below the threshold signal.

The nutational acceleration for a spin of 6 rps and a nutation frequency of 1 Hz is

$$4.5 \times 10^{-7} \text{ g/inch/degree}$$

The wide-band transducer can be integrated into the sphere so that its sensing center is approximately one inch from the sphere mass center. Thus, for 5 degrees of nutation the nutational acceleration will be approximately

$$2.25 \times 10^{-1} \text{ g}$$

so that the attenuation required to bring the nutational interference below the threshold of 10^{-6} g is

$$\text{Atten} = 20 \log \frac{2.25 \times 10^{-1}}{10^{-6}}$$

$$\text{Atten} = 20 \log 2.25 \times 10^5$$

$$= 107 \text{ db}$$

It is seen that an additional 95 db of attenuation must be provided at the frequency of 1 Hz. Two twin-T notch filters, shown in the figure, each providing 50 db of attenuation are used for this purpose.

5.4 Signal Conditioning

The TM system FM-FM sub-carrier oscillator requires an input voltage swing of 0-5 v. For this reason the amplifier output of ± 2.5 v must be off-set by 2.5 volts so that the signal zero is placed at +2.5 volts. Additionally, the voltage swing must not exceed -0.6 to +5.6 volts. This conditioning is provided by the system shown at the extreme right in Figure 6.

5.5 Structure Response Compensation

Because of the extended frequency range of the wide-band accelerometer the frequency response of the sphere and its internal structure (decks, brackets, components, and cabling) must be measured so that it may be combined with the accelerometer response to obtain the true response of the system to accelerations experienced by the skin of the sphere

To facilitate these measurements a test point is provided at the transducer output as shown at the extreme left in Figure 6. The test point is comprised of a long

shielded cable which, during the test, is passed through the clamp screw hole of the sphere. After completion of this test the cable is severed, its leads are shorted and the cable end is capped over with a metal shield.

As shown in Figure 7, the structure frequency response is measured by exciting the sphere along the direction of the wide-band accelerometer sensing axis (Z-axis) and then by simultaneous measurement of the acceleration levels at the exciter input and at the wide-band accelerometer as the frequency is swept over the specified spectrum. The exciter input level is measured by the use of a standard accelerometer that has a flat response well in excess of the spectrum of interest, and which is calibrated separately by the use of a microscope. The test is performed at a high level of acceleration in order to accommodate the sensitivity range of the standard and to produce signals well above the ambient seismic noise.

To improve the signal-to-noise ratio of the measurements, ambient noise is reduced by suspending the sphere on an elastic cord (bungee). This cord is made sufficiently long so that the input excitation is essentially a linear motion in the horizontal direction.

Conduction at the exciter input and at the base of the reference accelerometer is improved by the use of concave hemispherical metal pads coated with hard silicone grease.

Figure 8 shows the structure response curve, the wide-band accelerometer response curve, and the combined system

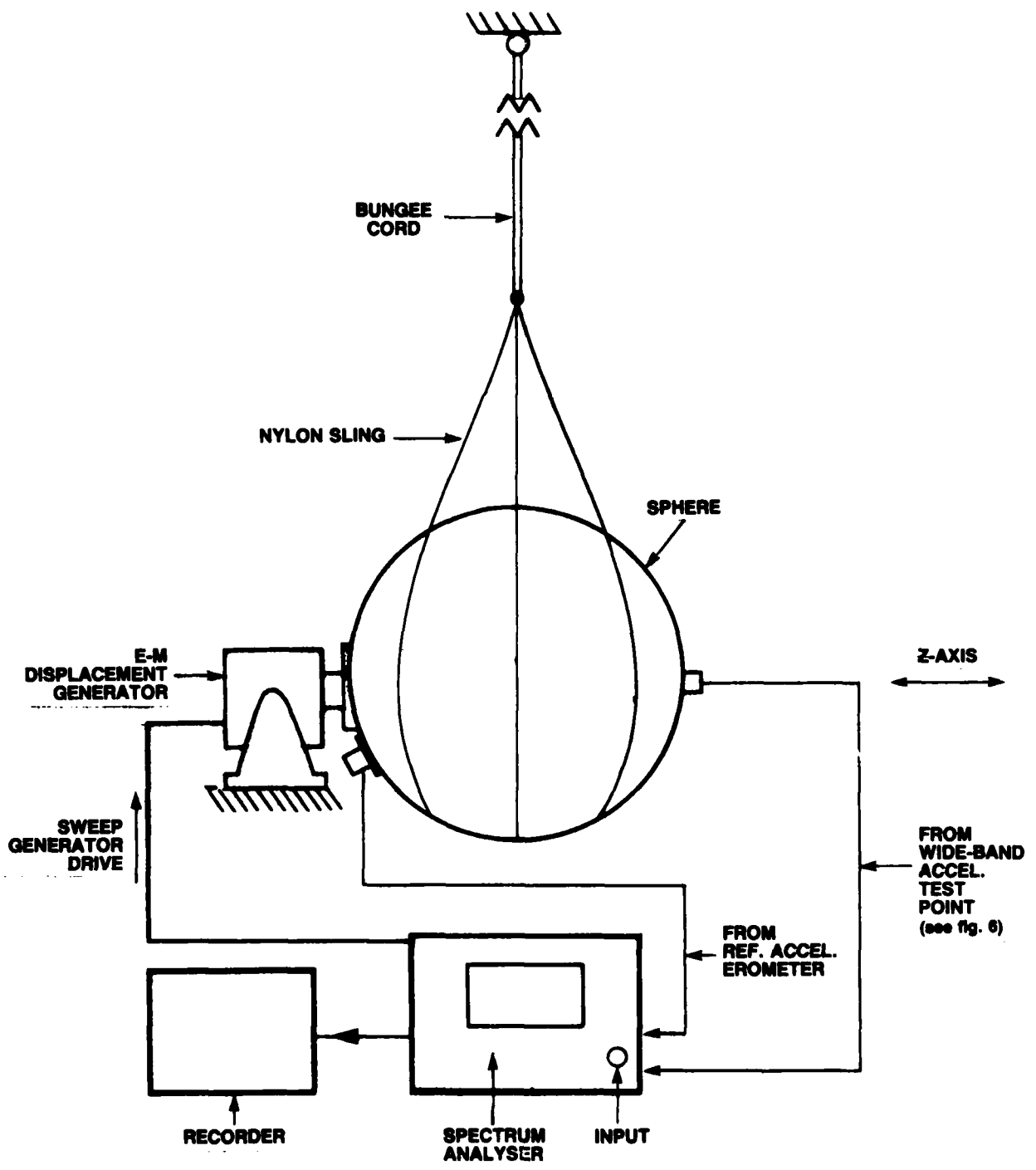

Structure Response Measurement
Figure 7

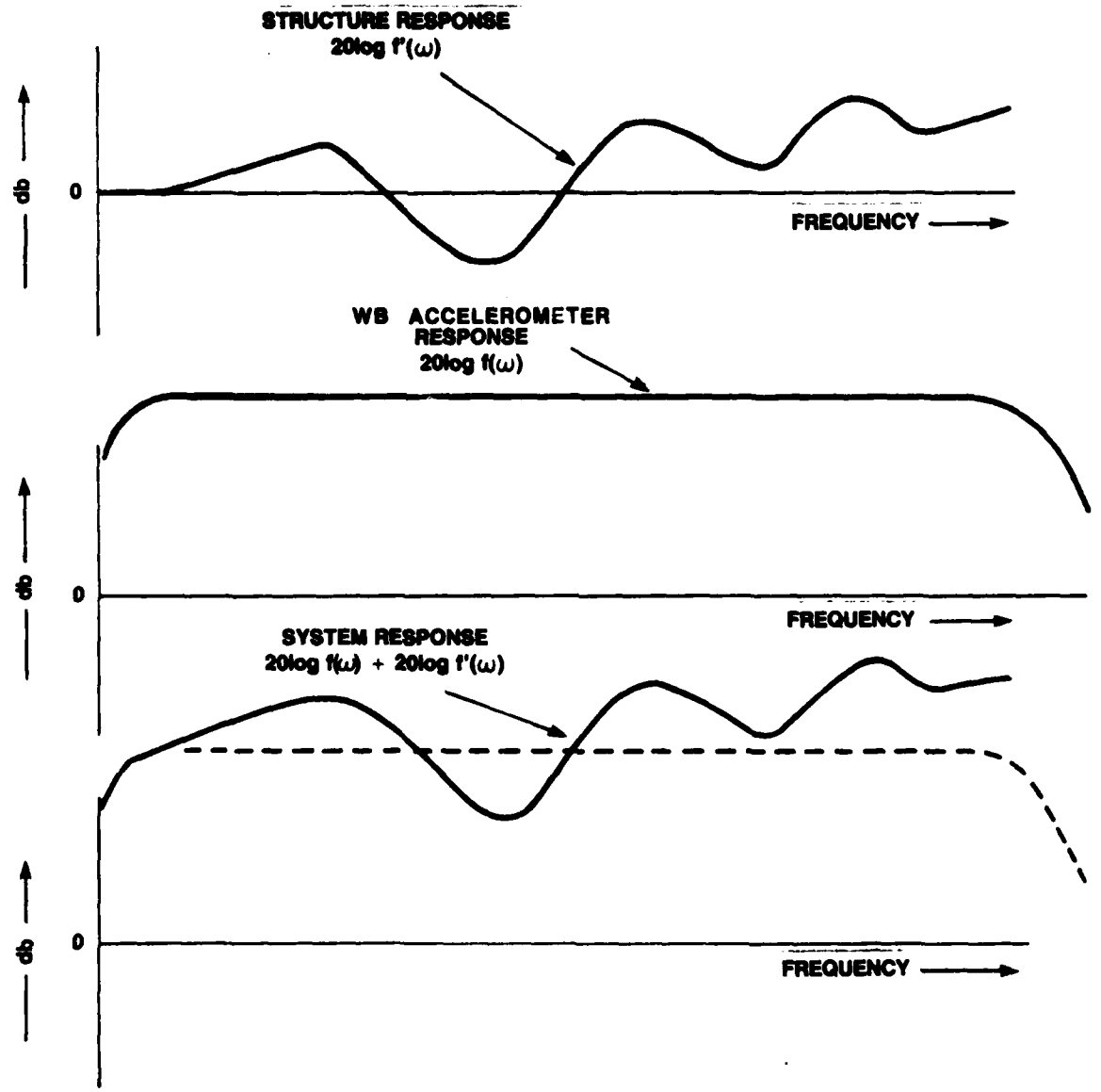

Wide-Band Response
Figure 8

response curve. It is noted that these data are in decibels so that the combining of the structure response and the accelerometer response curve is obtained by simply adding the ordinate values of these curves.

Let the structure response be expressed as

$$\frac{a_s}{a_{in}} = f'(\omega)$$

and the accelerometer sensitivity be expressed as

$$\frac{v_0}{a_s} = f(\omega)$$

The overall response is then

$$\frac{v_0}{a_{in}} = f(\omega)f'(\omega)$$

or, expressed in decibels

$$20 \log \frac{v_0}{a_{in}} = 20 \log f(\omega)f'(\omega)$$
$$= 20 \log f(\omega) + 20 \log f'(\omega)$$

It should be noted, also, that the structural affects at low frequencies are zero, i.e., the ratio of a_s/a_{in} is unity, or nearly unity. This is because the structure is sufficiently stiff at low frequencies so that when the sphere skin is displaced the structure displaces equally. This is not true at the higher end of the spectrum at frequencies approaching the structural natural frequencies where structural compliances are significant.

VI. NOSE CONE AND SPHERE EJECTION SYSTEMS

6.0 General

The tasks of fabrication, assembly, and testing of the nose cone and sphere ejection system have been consolidated with that of the sphere densitometer system. In addition to the economic advantages of this approach, there is the advantage of better efficiency in system trade-offs because all interacting systems are familiar to and in the control of one closely integrated group of personnel.

6.1 Nose Cone

The tasks involved in providing the nose cones for the payloads include the machining, fit-checking, and assembly of the component parts. Included also is the separation testing to insure a clean ejection of the nose-cone clam-shell sections. Two tests are performed: one at the laboratory using a band to retain the sections against their ejection springs which is abruptly released. This test will reveal any binding in the dove-tail joints of the two sections. The pyro wiring is checked out using dummy loads at the pyro terminals. This is followed by a test performed at AFGL using the flight configuration where the nose cone and support unit are tested as one system.

The nose cone is provided with fiber-glass slots to allow radiation from the sphere S-band transmitter during the ground check-out and launch phases of the mission. These slots had to be modified to accommodate the new antenna which was integrated into the sphere for the PCM-ranging system.

6.2 Sphere Ejection System

The sphere ejection system is comprised of a set of two rings which are fitted to the sphere around the top and bottom end cap segments. The bottom ring is free to translate several inches in the direction of the rocket spin vector and is loaded to produce this translation by the use of eight coil springs. The top ring is harnessed to the base frame of the system by three cables. Tensioning of these cables compresses the bottom ring against the coil springs. The top ring is in three equal segments held into position by a loop of cable which is passed through each of three guillotine pyros, one pyro to a segment, and lies in a groove cut into the O.D. of the composite ring.

Ejection of the sphere is accomplished by the initiation of the three pyros which cuts the loop cable allowing the spin centrifugal force to remove the top ring segments in a radial direction. The bottom ring is then free to be translated by the compressed coil springs. This ring thrusts uniformly against the bottom of the sphere imparting an impulse that results in a separation velocity of the sphere of approximately 4 m/sec.

The tasks involved in providing the sphere ejection system include the machining, fit-checking, and assembly of the component parts. The spring constants of the ejection springs are measured and paired to eliminate any imbalance in ejection thrust which may cause torquing which would cause undesirable free precession motion of the sphere.

Testing of this system involves the exercising of the translating ring to insure freedom and smooth actuation, and electrical checks of the cabling, using dummy loads to ascertain integrity of the pyro circuits. Later, the ejection system is tested at AFGL using the flight configuration but with a dummy sphere to check out the complete system using the support unit to initiate the pyros.

VII. MINI-SUPPORT UNIT

7.0 General

In the past each densitometer system has been accompanied by a separate array of sensors and a separate TM system, provided by others, for the purpose of monitoring the performance of the rocket. This equipment was housed in a payload section immediately behind the sphere section. This support section also provided timed discretes for the initiation of the pyrotechnic devices for the separation of the nose tip and for the ejection of the sphere.

Flight records have shown that essentially all the sensor information is duplicated in the sensor channels of the sphere S-band TM system, which operates from lift-off, and, hence, it was decided that the support unit need only provide the pyrotechnic timer and driver system, eliminating the support TM system and accompanying sensors.

7.1 Design

The electrical system is comprised of redundant systems for timing and supplying power discretes for the initiation of two Holex 5801 guillotines in the nose tip and three 5800 guillotines in the sphere ejection system. This system, shown in block form in Figure 9, uses two independent circuits each comprised of a Marathon 24-5113 Ni-Cad

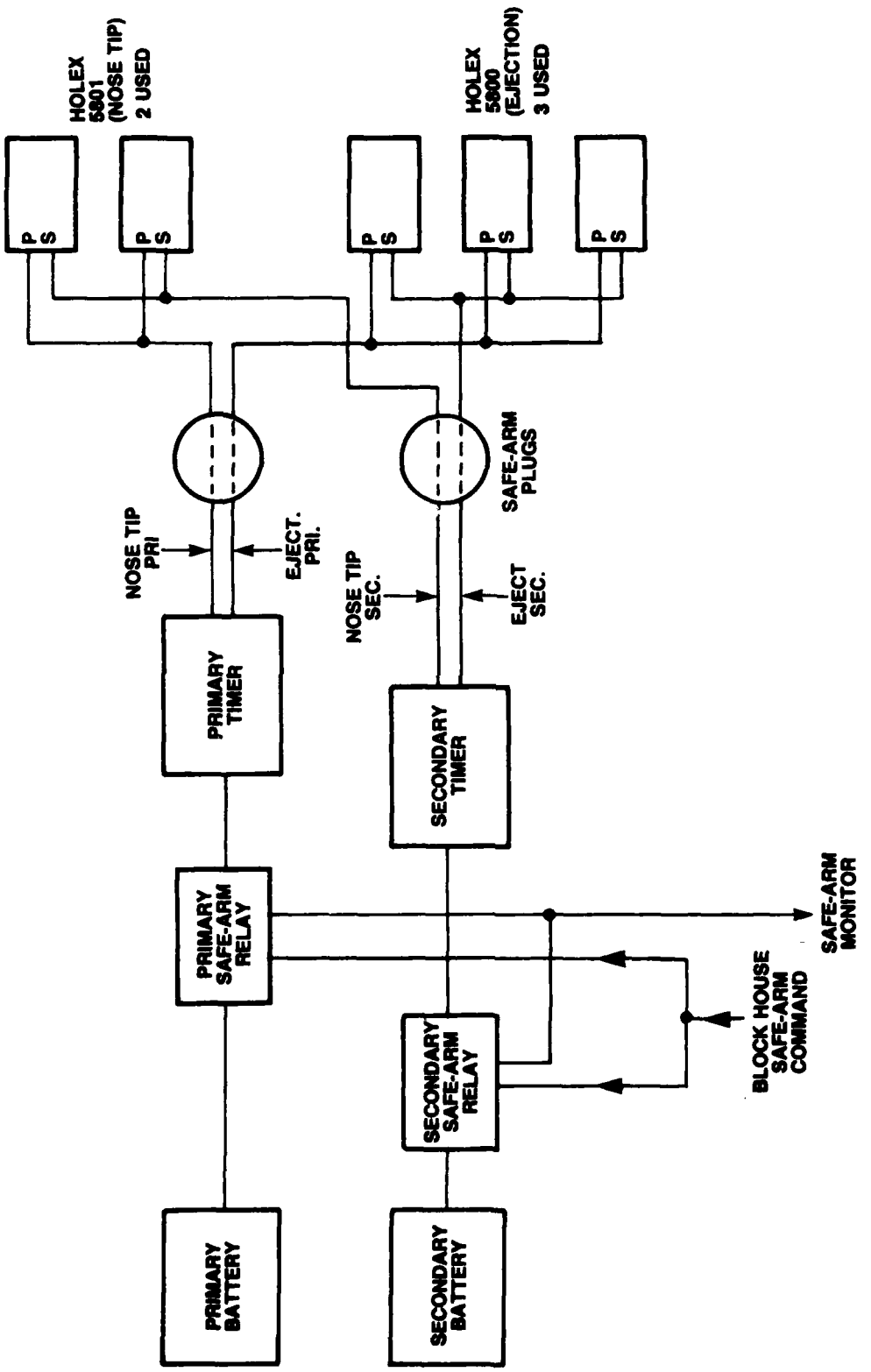

Pyro Timer and Driver System
Figure 9

battery, a Babcock BR23556 latching safe-and-arm relay, a Raymond Model 1060 interval timer, and Bendix connectors connected as safe-and-arm plugs; one cirtuit to supply all of the primary bridge wires in the pyros, the other to supply all the secondary bridge wires.

Each timer supplies two outputs, one output supplying a discrete to initiate the nose tip pyros and a few seconds later the other to supply initiation for the ejection pyros.

Two sets of safe-arm plugs are used. The "safe" pair provides shorts across the leads feeding the pyro busses while at the same time provides open circuits in the timer feed lines. The "Arm" pair provides jumpers to close the time-pyro circuits while at the same time provides a jumper to close the safe-arm relay command circuit.

The safe-arm relay command circuit is inter-locked, additionally, through the timer circuits so that the relay cannot be latched "on" unless the "arm" plugs are in position and the timers are rotated and latched. The condition of the safe-arm relays is monitored by lights on the block-house control box.

The remaining electrical system in the mini-support unit is the sphere umbilical interface connector, pyro lead connectors, and cabling, and the main umbilical connector which is mounted at a 45^{o} angle through the skin.

The system is packaged in a 12-inch diameter, 12-inch long can made of 1/4-inch E6061-6511 aluminum tubing which interfaces by means of a spigot joint to the aft end of the

densitometer payload section and by means of a similar joint to the forward section of the second-stage rocket. An internally mounted deck is placed midway across the diameter of the can onto which the component parts are mounted. An access door is provided for the safe and arm plugs and for timer winding and latching.

The inclusion of the mini-support unit in the overall densitometer development and fabrication task entailed the design and fabrication of umbilical cables to interface the payload with the launcher, blockhouse cables to interface the launcher with the control box, and the modification of the blockhouse control boxes to include the command and monitor circuits for the support unit. Additionally, a battery charger was designed and fabricated for trickle charging the pyro batteries.

VIII. SPHERE INTEGRATION

8.0 General

Several refinements in the sphere system which entailed the substitution of new sub-systems having different weights and dimensions has required the reintegration of the sphere in order to maintain balance and second-moment trim while at the same time keeping control over the system total launch weight. These refinements included the installation of a more-powerful transponder, a ten-bit encoder to replace the eight-bit unit formerly used, and the provision for accommodating a new PCM-ranging system for use at rocket ranges where ground equipment is unavailable for transponder-augmented radar tracking.

8.1 Transponder

The smaller and lower-powered Vega Model 349C-4 transponder has been replaced by the Vega Model 366C. This change required the provision of a greater volume of space beneath the main deck. This was possible only by the repackaging of the Power Control Unit, which shares the below-deck space, to obtain a narrower form-factor. Balance was partially compensated by the removal of battery cells, formerly mounted below the main deck, to positions above the deck.

8.2 Encoder and PCM Ranging

The formerly-used eight-bit encoder has been replaced by a new ten-bit encoder designed and fabricated by OSURF. The new unit houses the DC-DC converter which was mounted externally on the sub-deck in past designs. This new encoder has different mounting provisions and a different weight. This was accommodated by relocating the mounting holes in the arch structure and by enlarging the sub-deck cut-outs, and by shifting other components slightly for balance compensation.

Provision had to be made for the sub-carrier oscillators which are required for the wide-band accelerometer and, when used, the PCM-ranging system.

The PCM-ranging system is comprised of a WTA Model R104N receiver, having a weight approximately one-third that of the transponder, and an additional SCO of insignificant weight. Because this system trades places with the transponder, depending upon the rocket-range ground equipment, those spheres integrated with PCM ranging have two battery cells placed below the main deck to help maintain balance.

IX. INTEGRATION STUDIES

9.0 General

Because of the increased total weight imposed upon the sphere by the addition of the new transponder and the wide-band accelerometer it was decided that some effort should be expended on a re-appraisement of the mechanical design of the sphere so that in the future the design may be modified to achieve weight reduction. A corollary to this effort would be the attainment of a better configuration to obtain additional volume for future system additions.

Configuration changes to reduce weight are constrained by static balance, moment-of-inertia requirements, and the maintenance of proper heat flow to control temperature. Ease of assembly and accessibility of sub-systems are important considerations.

9.1 Configuration

The two spherical end caps and the antenna band of the present configuration are secured into one assembly by the use of an internal arch which is bolted to the lower end cap at its two ends and which extends upwards so that its apex coincides with the inside center point of the upper end cap. The central area of the upper end cap is reinforced with a large internal boss through which a large bolt is passed to engage with a tapped hole in the arch. The torquing of this

bolt draws both end caps into intimate contact with the antenna band.

Because of the inherent strength of the spherical shape and because of the thickness of the aluminum used in the design of the end caps and antenna band, these parts may be secured by the use of eight small screws, as shown in Figure 10, which are passed through the edge of the antenna to engage with tapped holes in the lip of the end caps. This is demonstrated by comparing the stress carrying ability of the smaller screws with the one large bolt. If the metal used in the fasteners is identical (stainless steel) the safety factor of the new method of fastening is simply the ratio of the screw cross-section areas

$$\text{Safety Factor} = \frac{8 \times \text{Area (small screws)}}{\text{Area (bolt)}}$$

A No. 4 screw is selected for the new design which has a diameter of 0.112 inches. The existing clamp bolt has a diameter of 0.312 inches, thus

$$SF = \frac{8d^2}{d^2} = \frac{0.1}{0.097} = 1.031$$

An additional factor of two can be applied to this factor because the new design the screw loading is in shear as compared to the tension loading of the old design.

Elimination of the arch structure will reduce the sphere weight by 1.07 lbs. Additional weight savings can be achieved by changing the metal used in the deck stand-off

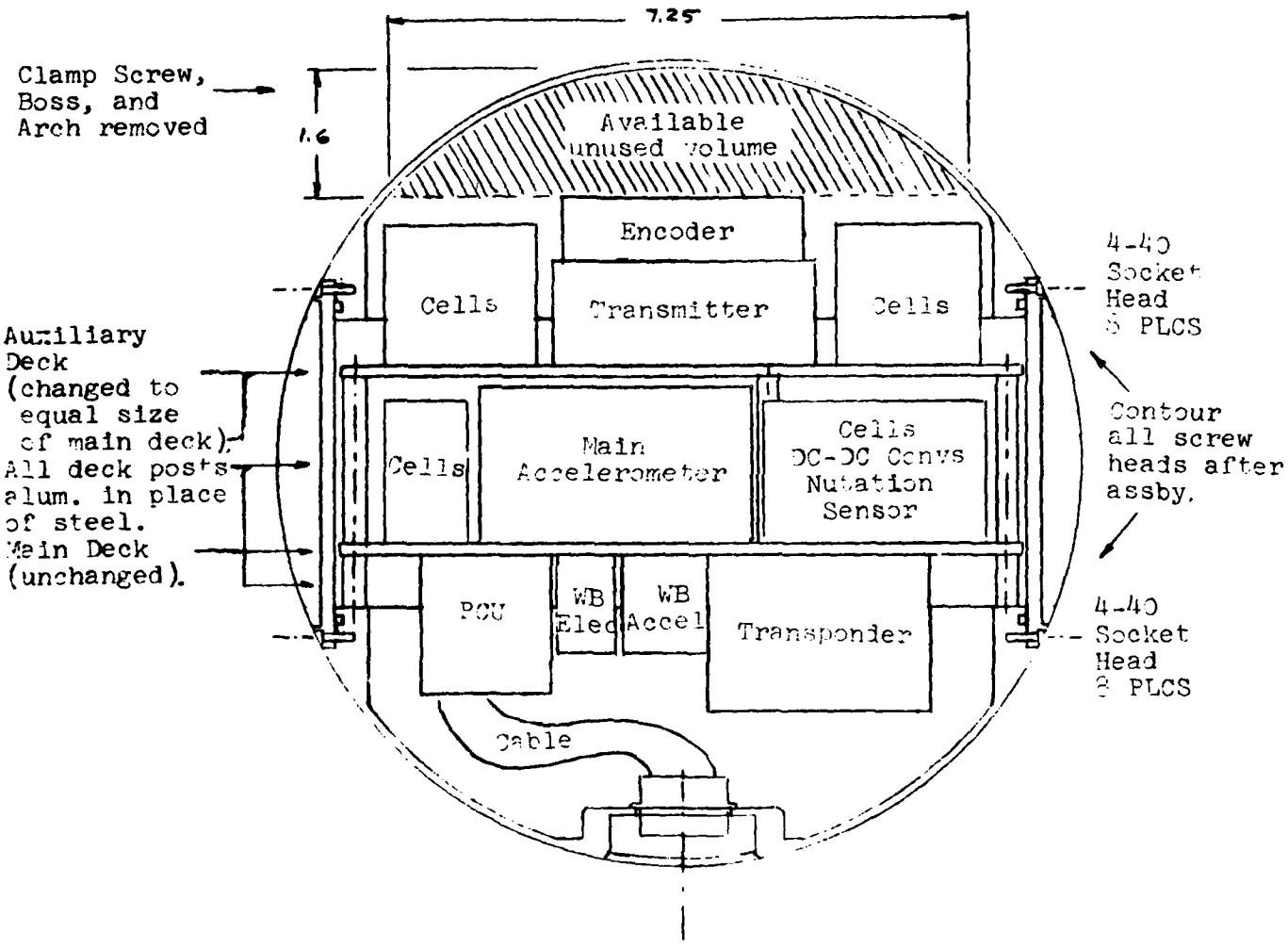

FIGURE 1)

REV LET	DESCRIPTION	CH'K BY & DATE	ENG APPR.
DO NOT SCALE FOR CONSTRUCTION			
TOLERANCES UNLESS OTHERWISE SPECIFIED FRACTIONAL: UP TO 24" ± 1/64, OVER 24" ± 1/32 DECIMAL: XX ± .01, XXX ± .005 ANGULAR: DEGREES ± 1/2°, MINUTES ± 5' FINISH 63 RMS MICROIN CONCENTRICITY .005 TIR			

PART NO.	NO REQ'D	DESCRIPTION	MAT'LS & SPECIFICATIONS

	APPROVED	DATE
DESIGN ENG		
PROJ ENG		
MFG		
PART REQ'D BY		
MFG BY		

ACCUMETRICS CORPORATION
344 RINDGE AVENUE
CAMBRIDGE, MASS 02140
617 868-1142

TITLE: 10-INCH SPHERE PROPOSED CONFIGURATION

REF DWG.

PROJ. 81-1

DR BY	DATE	CH'K BY	DATE

SCALE

D100130

supports from steel to aluminum. However, this will be off-set by the increased weight of the larger auxiliary deck used in the new configuration.

The fore-shortened auxiliary deck presently used will be extended to equal the area of the main deck which remains unchanged. Because of the larger span of the auxiliary deck an additional support stand-off will be located in an unused space near its center which will serve to structurally tie the two decks together in this area.

Balance and inertia trim will be maintained by moving some of the battery cells to the auxiliary deck as shown in Figure 5.

As shown in the figure, a spherical segment of volume having a diameter of 7.25 inches and a height of 1.6 inches plus certain smaller restricted volumes projecting downward from this volume is available for additional instrumentation. For the same total weight as the existing sphere configuration the weight allowance for additional instrumentation would be 1 lb.

9.2 Heat Flow

The transmitter is the important heat producing component in the sphere system. It is presently mounted onto the arch with conductive heat flow paths to the lower end cap of approximately 2 inches in length. The cross-section area of each leg of the arch is 0.15 in^2. The transmitter will be placed on the auxiliary deck of the new design so that the heat flow path will radially directed

through the deck to the deck support posts and then to the lower end cap. Because the cross-section area of the radial path through the deck is large it is only important to consider the paths conducting heat from the deck to the lower end cap through the deck support posts. These posts are 2 inches long and, hence, the length of the path and material is the same as the present configuration so that only the cross-section area requirement of the posts need be calculated. The area of the existing design is 0.3 $in.^2$ If the post diameter is fixed at 0.25 in the area required for the posts would be N x 0.0491 where N is the number of posts, thus

$$N = \frac{0.3}{0.0491} \simeq 6$$

Since 10 posts are required for mechanical strength it is seen that the new configuration provides for a more efficient conductive transfer of heat to the outside of the sphere.

In addition, the large deck upon which the transmitter is mounted will provide better convective flow. To reduce convective coupling into the main accelerometer a thin sheet of styrofoam may be required between the top of the accelerometer and the auxiliary deck.

9.3 Battery Energy Reserve

Any future expansion of the sphere instrumentation system must include consideration of the energy storage capability of the present battery. If the new ampere-hour requirement exceeds this capability a new battery would

have to be designed and integrated into the sphere made up of larger-sized cells. This follows because the ampere-hour capacity of a battery is determined by the series elements comprising the battery or by the size of the cell in the case of the sphere system.

The sphere uses a battery consisting of 23 Power, Inc. Model 1200SCL nickel-cadmium C-cells. Fully charged this battery produces a terminal voltage under load of approximately 30 volts. This voltage decreases in the first 5 minutes of full-load operation to 27 volts where it levels off for a duration depending upon the load current. After this period it falls again rapidly. The sphere system will operate satisfactorily with a supply voltage in the range 25 to 30 volts.

The total current requirement for the transponder-equipped sphere is 1.65 amperes. With this load the battery will maintain a supply voltage within the operating range for 20 minutes. For the sphere equipped with the PCM-ranging system the total load current is 1.3 amperes. With this load the battery voltage will stay within the operation range for 35 minutes.

For a typical mission the combined internally-powered and flight time after the last battery charging opportunity is approximately 15 minutes. Based on this time interval the battery supply voltage would be within the operating range for a total load current not exceeding 2.2 amperes. For the two different configurations this would represent

energy reserves of

Sphere with Transponder:

$$(2.2 - 1.65)15 = 8.25 \text{ amp/min}$$

Sphere with PCM-ranging:

$$(212 - 1.30)15 = 13.5 \text{ amp/min}$$

or load current margins, based on the 15-minute internal power operating time, of

Sphere with Transponder: 0.55 amperes

Sphere with PCM-ranging: 0.90 amperes.

These currents represent the maximum allowable additional loads for any future expansion in the sphere instrumentation.

X. FLIGHT TESTING

10.0 General

The four densitometer systems developed on this contract were launched as follows:

AC-11 White Sands Missile Range, on 14 August 1979

Ac-12 ESRANGE, Kiruna, Sweden, on 15 November 1980

AC-13 ESRANGE, Kiruna, Sweden, on 30 November 1980

AC-14 Poker Flat Rocket Range, Fairbanks, Alaska, on 6 March 1981

Unlike with former launches the field support for these payloads was extended to include the preparation and check-out of the nose tip and ejection system in addition to the preparation and check-out of the spheres.

AC-11 at WSMR did not achieve altitude because of a failure in the ignition system of the rocket. The AC-14 flight data revealed an error in the Y-axis data indicating a fracture in the Y-axis transducer element. Because of the redundancy inherent in the design this did not overly degrade flight performance.

AC-12 and 13 performed satisfactorily in flight, however, the accelerometer in AC-13 uncaged during pre-flight check-out due to a failure in the timing circuit controlling the squib firing. The accelerometer was recaged and the timer circuit was replaced with a back-up

unit, AC-13 was then launched and performed satisfactorily.

10.1 White Sands Field Trip (AC-11)

A field trip was made to the White Sands Missile Range covering the period 6 August to 15 August, 1979 for the purpose of launching Densitometer No. AC-11. No problems were encountered during build-up and check-out. This system was launched on 14 August 1979 but did not achieve altitude because of a failure in the second-stage rocket ignition system. Telemetry data indicated that all payload pyrotechnics fired at the proper times and that the accelerometer was performing normally.

10.2 Esrange, Kiruna, Sweden Field Trip (AC-12, AC-13)

A field trip was made to Esrange, Kiruna, Sweden covering the period 24 October to 5 December, 1980 for the purpose of the launching of Densitometers AC-12 and AC-13. No problems were encountered in the build-up and check-out of AC-12. This system was launched on 15 November 1980 and it performed satisfactorily.

No problems were encountered during the build-up of AC-13, however, during pre-launch check-out a transistor failed in the time-circuit located in the Power Control Unit. This caused the accelerometer uncaging squibs to fire and uncaging of the proof masses resulted. The unit was disassembled and the back-up Power Control Unit was installed in place of the faulty unit. The accelerometer was recaged and the payload was rehung on the rocket.

AC-13 was then launched on 30 November 1980 giving satisfactory performance in flight.

10.3 Poker Flat, Fairbanks, Alaska Field Trip (AC-14)

A field trip was made to the Poker Flat Rocket Research Range, Fairbanks, Alaska covering the period 18 February to 7 March 1981 for the purpose of launching Densitometer No. AC-14. No problems were encountered during the build-up and check-out of this payload.

AC-14 was launched on 6 March 1981 and performed satisfactorily. Post-flight examination of the data revealed a shift in the natural frequency of the Y-axis transducer. Additionally, its output amplitude appeared to have degraded when compared to the X-axis output. Further examination of pre-flight calibration data indicated that the piezo-electric element was faulty. However, because of the redundancy inherent in the X- and Y-axis systems this malfunction did not overly degrade the flight data.


DA
FIL